



Intimate contact of enolic species with silver sites benefits the SCR of NO_x by ethanol over Ag/Al₂O₃

Yong Yan, Yunbo Yu*, Hong He, Jiaojiao Zhao

Research Center for Eco-Environmental Sciences, Chinese Academy of Sciences, Beijing 100085, China

ARTICLE INFO

Article history:

Received 16 November 2011

Revised 22 May 2012

Accepted 29 May 2012

Available online 12 July 2012

Keywords:

Selective catalytic reduction of NO_x

Enolic species

Ag/Al₂O₃

Acetate

Isocyanate

ABSTRACT

Alumina-supported silver (Ag/Al₂O₃) catalysts with different silver loadings were investigated for the selective catalytic reduction of NO_x by ethanol. The catalytic role of silver in the formation of enolic species was studied by ultraviolet–visible spectroscopy, diffuse reflectance infrared Fourier transform spectroscopy combined with mass spectrometry, density functional theory calculations, and kinetic measurements. It was found that the enolic species originating from the partial oxidation of ethanol over Ag/Al₂O₃ prefer to adsorb on or close to silver sites, in intimate contact with the active phase. This adsorption behavior of this enolic species contributes to its high activity for the formation of isocyanate species (–NCO) and the final product N₂ during the NO_x reduction by ethanol over Ag/Al₂O₃. Surface acetate also formed during this process, while only interacting with Al sites, resulting in a lower activity for –NCO formation. Meanwhile, the mechanism of the NO_x reduction by ethanol was discussed.

© 2012 Elsevier Inc. All rights reserved.

1. Introduction

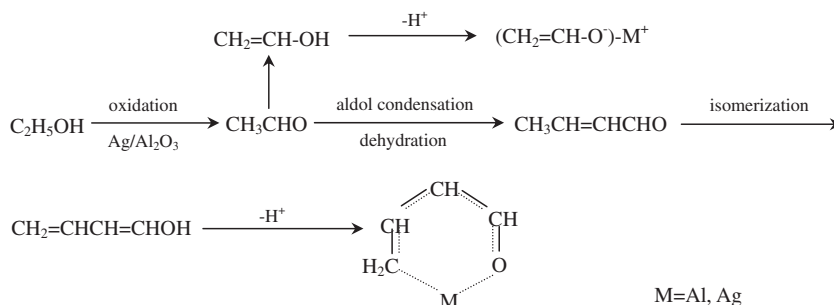
Selective catalytic reduction (SCR) of NO_x in the oxygen-rich exhaust emission from lean burning engines remains one of the major challenges for environmental catalysis. Since the pioneering work of Iwamoto et al. [1] and Held et al. [2], many catalysts such as zeolitic oxide, base oxide/metal and noble metal catalysts have been found to be effective for the SCR of NO_x by hydrocarbons (HC–SCR) in the presence of excess oxygen [3–11]. Among them, Ag/Al₂O₃ is known as one of the most effective catalysts for HC–SCR [4–5,11–22]. When using oxygenated hydrocarbons as reductants, particularly ethanol, Ag/Al₂O₃ shows high activity even in the presence of SO₂ and H₂O [23].

To improve the overall performance of Ag/Al₂O₃ for NO_x reduction, much effort has been devoted to gaining insight into the reaction mechanism. Generally, the SCR of NO_x by ethanol can be considered as follows: NO + O₂ + C₂H₅OH → NO_x (adsorbed nitrate in particular) + ad-C_xH_yO_z → R–ONO + R–NO₂ → –NCO + –CN → N₂ [13,14,18–20,24–26]. Nevertheless, many questions remain regarding the details of this multi-step process. It has been proposed that acetate derived from the partial oxidation of ethanol plays a crucial role in the formation of isocyanate species (–NCO), as well as in the global NO_x reduction process [4,18,20,25]. From our previous research, large amounts of surface enolic species were observed by in situ diffuse reflectance infrared Fourier transform spectroscopy (DRIFTS) during both the partial oxidation of ethanol

and reduction of NO_x with ethanol over Ag/Al₂O₃, which was further confirmed by density functional theory (DFT) calculations [5,27–29]. The formation of adsorbed enolic species on the Ag/Al₂O₃ surface has been proposed as following: ethanol principally reacts with oxygen to form acetaldehyde, which is followed by isomerization to ethenol. Additionally, an enolic anion (CH₂=CH–O[–])–M⁺ is formed by hydrogen extraction when ethenol is adsorbed on the surface of Ag/Al₂O₃. Meanwhile, the possible occurrence of aldol condensation of acetaldehyde may lead to the formation of C₄ enolic species as shown in Scheme 1 [29]. The surface enolic species exhibited much higher activity in reaction with nitrate and/or NO + O₂ to form –NCO species than that of acetate, demonstrating its crucial role in the SCR of NO_x by ethanol. More recently, the enolic species was also clearly observed by Kim et al. [30] and found to contribute to the reduction of NO_x by ethanol over Ag/Al₂O₃. Previous research further identified that enolic species also play a key role in the reduction of NO_x by other alcohols (1-propanol, isopropyl alcohol, 1-butanol, sec-butyl alcohol, and isobutyl alcohol) over Ag/Al₂O₃ [31–34], acetaldehyde over both Ag/Al₂O₃ [27] and Co/Al₂O₃ [35], and acetylene over ZSM-5 [36]. Interestingly, substantial quantities of enols in the gas phase have been observed by photoionization mass spectrometry during the combustion of hydrocarbons [37]. The above results strongly suggest that adsorbed enolic species and/or enols in the gas phase are common intermediates involved in the partial oxidation of hydrocarbons, oxygenated hydrocarbons, and NO_x reduction. Based on this, a new mechanism via enolic species formation followed by transformation to –NCO species has been proposed for the reduction of NO_x by alcohols such as ethanol, which can be

* Corresponding author. Fax: +86 10 62849121.

E-mail address: ybyu@rcees.ac.cn (Y. Yu).



Scheme 1. The pathway for the surface enolic species formation during the partial oxidation of ethanol on Ag/Al₂O₃.

simply described as: $\text{NO} + \text{O}_2 + \text{C}_2\text{H}_5\text{OH} \rightarrow \text{NO}_x$ (nitrate in particular) + $\text{C}_x\text{H}_y\text{O}_z$ (enolic species in particular) $\rightarrow \text{R}-\text{NO}_2 + \text{R}-\text{ONO} \rightarrow -\text{NCO} + -\text{CN} \rightarrow \text{N}_2$ [5,28,31,34,38]. This mechanism successfully explained the higher efficiency for the SCR of NO_x by ethanol if compared with the reduction of NO_x by propene or methanol over Ag/Al₂O₃ [28,32]. This mechanism also explained the differing influence of water vapor on the SCR of NO_x by ethanol or by propene, which has confused us for a long time [5].

Meanwhile, many studies focused on the relationship between the structural features of Ag/Al₂O₃ catalysts and their catalytic activity for the SCR of NO_x. It is widely accepted that NO_x reduction is strongly correlated to silver loading. Structural characterization, particularly by Ultraviolet–visible spectroscopy (UV–vis), X-ray adsorption spectroscopy (XAS), and X-ray photoelectron spectroscopy (XPS) measurements, identified that oxidized silver was predominant on Ag/Al₂O₃ catalysts with moderate silver loading, whereas metallic silver clusters (Ag_n⁰) became dominant on high-silver content alumina catalysts [21,30,39–44]. Generally, oxidized silver present as isolated Ag⁺ cations and/or oxidized silver clusters (Ag_n^{δ+}) on the Al₂O₃ surface are responsible for the HC–SCR reaction, while metallic silver clusters are responsible for the direct combustion of hydrocarbons at the expense of NO_x reduction [27,40–45]. More recently, Nam and co-workers [22,30] proposed that Ag⁺ and Ag_n^{δ+} are active for the reduction of NO_x by diesel fuel–ethanol mixtures and *n*-dodecane, while metallic Ag is responsible for the partial oxidation of hydrocarbons, which promotes the initiation of the HC–SCR process in the low temperature range. This result indicates that an optimal ionic/metallic ratio of Ag species on Al₂O₃ surface is probably needed, which is in agreement with the result of Pârvelescu et al. [21].

On a detailed mechanistic level, the role of silver species in the HC–SCR of NO_x over Ag/Al₂O₃ was mainly attributed to enhancement of the partial oxidation of reductants to form active species, promotion of the formation of key intermediates such as –NCO, and their further reaction to produce N₂ [5,23,27,46]. As described above, the enolic species adsorbed on the Ag/Al₂O₃ surface plays a crucial role in the SCR of NO_x by ethanol. Furthermore, the formation of enolic species is the main reason why the activity of Ag/Al₂O₃ for the reduction of NO_x by propene is higher than that of the Cu/Al₂O₃ [38], indicating that silver could play a key role in the formation of enolic species. Up to now, however, there is little information focusing on this point.

In this paper, the catalytic role of silver in the formation and reactivity of enolic species during the SCR of NO_x by ethanol on Ag/Al₂O₃ with different Ag loadings were studied by kinetic measurements, in situ DRIFTS and DFT calculations. It was found that the enolic species selectively adsorbed on or close to silver sites, while surface acetate was prone to adsorb on Al sites, which may account for their different activity and role in the reduction of NO_x by ethanol over Ag/Al₂O₃.

2. Experimental

2.1. Catalysts preparation and characterization

As described in our earlier paper [5], Ag/Al₂O₃ catalysts with different loadings (2, 4, and 8 wt%) were prepared by an impregnation method, immersing boehmite into an aqueous solution of silver nitrate. After impregnation, the excess water was removed in a rotary evaporator at 333 K. And then the sample was calcined in air at 873 K for 3 h. The treatment method for pure γ-Al₂O₃ material was similar to that of the Ag/Al₂O₃ catalysts. To remove the metallic silver clusters and weakly bound silver species, the 4 wt% Ag/Al₂O₃ was immersed in 10% HNO₃ for 10 h, which was followed by calcination at 723 K and 873 K for 3 h in N₂ (denoted as 4wt% Ag/Al₂O₃-L thereafter) [43]. The real content of Ag in the parent and leached samples was measured by ICP analysis (Plasma Quad 3, VG Co., England).

UV–vis diffuse reflectance spectra were collected at room temperature in air with BaSO₄ as a reference (U-3100 UV–vis spectrophotometer, Hitachi Co., Japan). All spectra were measured in the range of 190–820 nm with a resolution of 2 nm. Considering that the Al₂O₃ support exhibited strong absorbance below 300 nm [44], the spectrum of bare alumina was subtracted from the spectra of Ag/Al₂O₃ catalysts to better understand the UV–vis results [30].

2.2. Reaction rate measurements

The kinetic measurements were carried out in a fixed-bed reactor by passing a gaseous mixture of NO (800 ppm), C₂H₅OH (1565 ppm), water vapor (10%), and O₂ (10%) in N₂ balance at a total flow rate of 1000 mL min⁻¹ (GHSV = 300,000 h⁻¹). An aqueous C₂H₅OH solution was supplied into the gas stream with a micro-pump and vaporized by a coiled heater at the inlet of the reactor. The concentrations of NO and NO₂ in the inlet and outlet gases were analyzed online by an FTIR spectrometer (Nicolet Nexus is10) equipped with a gas cell of volume 0.2 dm³. In this case, the gas cell of the FTIR spectrophotometer and the gas line after the reactor were heated to 120 °C to avoid water condensation. The spectra were collected with a resolution of 0.5 cm⁻¹ and with an accumulation of 16 scans when the SCR process reached a steady state (after reaching the desired temperature for 60–120 min). The tests were carried out three times for each case under the same conditions. To realize a differential reactor assumption, the NO_x conversion was kept below 10% over the whole tested temperature region (from 450 K to 575 K). Also, the mass transport effect was eliminated by using samples with a particle size of 0.45–0.9 mm under a total flow rate of 1000 mL/min, which was confirmed by corresponding experiments (see Supplementary information and Fig. S1). N₂O, NH₃, and CO, as by-products of HC–SCR, were

measured simultaneously by the FTIR spectrometer. In our case, the concentration of N_2O was negligible during the reduction of NO_x by ethanol over Ag/Al_2O_3 , and the detected amount of NH_3 was about 15 ppm. Based on this, NO_x conversion to N_2 was calculated using the following equation:

$$NO_x \text{ conversion to } N_2 = \frac{[NO]_{in} - [NO]_{out} - [NO_2]_{out} - [NH_3]_{out}}{[NO]_{in}} \times 100\%.$$

Meanwhile, a relationship between N_2 production and CO formation over 4 wt% Ag/Al_2O_3 at 673 K was obtained (Fig. S2), which was used to estimate the concentration of N_2 during the mass measurement (in Section 2.3).

In accordance with the literature [43], the rate of NO_x conversion to N_2 ($-r_{NO_x}$) is determined as follows:

$$-r_{NO_x} = F_{NO_x} X_{NO_x} / W \text{ (mol/g/s)},$$

where W is the weight of catalysts, F_{NO_x} is the molar flow rate of NO_x (mol/s), and X_{NO_x} is the conversion of NO_x to N_2 . Reaction rates, normalized by the surface area, were calculated by dividing these rates by the initial specific surface area of each sample. Apparent activation energies were calculated from Arrhenius-type plots of the reaction rate.

The corresponding turnover frequency (TOF) was calculated by dividing the rate of NO_x reduction by the amount of accessible silver species measured by H_2-O_2 titration [47]. This measurement was performed on an Automated Catalyst Characterization System (Autochem 2920, Micromeritics, USA) equipped with a TCD detector, using 100 mg catalyst powder. Prior to the titration procedure, the samples were pretreated at 573 K for 0.5 h in a flow of 5 vol.% O_2/He (50 mL/min) and cooled down to room temperature. The samples were then exposed to a flow of 10 vol.% H_2/Ar (50 mL/min), raised to 523 K (10 K/min), and maintained for 2 h, followed by cooling down to 443 K in He flow. After this, the feeding gas was changed sequentially to 5% O_2/He (50 mL/min) for 1 h and then purged with Ar for another 2 h. Finally, the adsorbed oxygen was titrated by introducing pulses of hydrogen (25 ml per pulse), which was further analyzed to determine the amount of accessible silver species (1 mol H_2 consumption indicates 2 mol accessible silver metal).

2.3. In situ DRIFTS experiments

In situ DRIFTS spectra were recorded on a Nexus 670 (Thermo Nicolet) FT-IR, equipped with an in situ diffuse reflection chamber and a high sensitivity MCT/A detector. Ag/Al_2O_3 catalyst and pure $\gamma-Al_2O_3$ material (ca 20 mg) for the in situ DRIFTS studies were finely ground and placed in ceramic crucibles in the in situ chamber. Mass flow controllers and a sample temperature controller were used to simulate the real reaction conditions, such as mixture of gases, pressure, and sample temperature. Prior to recording each DRIFTS spectrum, the sample was heated in situ in 10% O_2/N_2 (or Ar balance) flow at 873 K for 1 h and then cooled to the desired temperature to measure a reference spectrum. All gas mixtures were fed at a flow rate of 300 ml/min. All spectra were measured with a resolution of 4 cm^{-1} and with an accumulation of 100 scans.

The composition of the outlet gas from the in situ IR chamber was also continuously monitored using a quadrupole mass spectrometer (HPR20, Hiden Analytical Ltd.). Typically, the following mass-to-charge (m/e) ratios were recorded as a function of time on stream: NO ($m/e = 30$), CO_2/N_2O ($m/e = 44$), N_2/CO ($m/e = 28$) and N^{14} ($m/e = 14$). Quantification was carried out with reference to the NO signal. Our FTIR measurement with the gas cell confirmed that N_2O ($m/e = 44$) formation was negligible during the reduction of NO_x by ethanol over Ag/Al_2O_3 . Thus, the mass signal at $m/e = 44$ was used as an indicator of CO_2 . The formation of N_2

originating from surface reaction was calculated based on the signal at $m/e = 28$ after deducting the contribution of CO to $m/e = 28$, with the assumption that the concentration of CO is 2.6 times the production of N_2 (Fig. S2).

2.4. DFT calculations

DFT calculations were used to confirm the structure of adsorbed enolic species on pure Al_2O_3 using the GAUSSIAN 09 suite of programs. The LANL2DZ basis set was employed to carry out the DFT-B3P86 (Becke's 3-parameter function with a non-local correlation provided by the Perdew 86 expression) calculations [28].

3. Results

3.1. Catalyst characterization

In our previous study [5], Ag/Al_2O_3 catalysts with different Ag loadings were characterized by BET and XRD measurements. Pure Al_2O_3 exhibited a BET surface area of $292.1 \text{ m}^2/\text{g}$ (Table 1). An increased silver loading from 2 wt% to 8 wt% results in a gradual decrease in the surface area, giving values within the range of $239.8-209.9 \text{ m}^2/\text{g}$. The BET surface area for 4 wt% Ag/Al_2O_3-L is $236.4 \text{ m}^2/\text{g}$, which is similar to that of the parent samples of 4 wt% Ag/Al_2O_3 . XRD patterns of Ag/Al_2O_3 catalysts showed that only the $\gamma-Al_2O_3$ phase was detected as the silver loading increased from 2 to 4 wt%, but the metallic Ag and Ag_2O phases were observed on 8 wt% Ag/Al_2O_3 . ICP analysis (Table 1) showed that the real contents of Ag in the parent samples were close to the nominal values. On the leached sample of 4 wt% Ag/Al_2O_3 , the Ag content was 0.53%, confirming that large amounts of Ag species were effectively removed by HNO_3 leaching.

UV-vis analysis was further used to identify the state of silver supported on Al_2O_3 in this study, with the results shown in Fig. 1. Peaks appearing at 230 and 260 nm can be assigned to highly dispersed silver ions (Ag^+) and oxidized silver clusters (Ag_n^{2+}), respectively, while bands located at 290 and 350 nm are due to metallic silver clusters (Ag_n^0) [30,44,48]. To compare the quantity of these silver species on Ag/Al_2O_3 with different silver loadings, the UV-vis spectra were further deconvoluted into Gaussian subbands on the basis of our assignment, and then the percentage of different silver species was calculated by analysis of the integrated peak area. The results listed in Table 2 show that Ag species are mainly present in the oxidized state, particularly as highly dispersed Ag^+ ions on all Ag/Al_2O_3 samples, even with Ag loading up to 8 wt%. A similar result was also observed on fresh 10 wt% Ag/Al_2O_3 [49], where the ratio of Ag^+ ions was 71.5%.

It has been reported that UV-vis spectra cannot provide a quantitative picture of the state of Ag on Al_2O_3 for the following reasons: (1) strong absorbance of the Al_2O_3 support below 300 nm; (2) extremely high extinction coefficients for Ag_n^{2+} and Ag_n^0 clusters compared with that of Ag^+ ions; (3) the "invisibility" of UV-vis spectroscopy for some types of Ag^+ ions reflected in the region

Table 1

The real silver content, BET surface area, and H_2 consumption of Ag/Al_2O_3 with different silver loadings.

Sample	Silver content (wt%) ^a	BET surface area (m^2/g)	H_2 consumption ($\mu\text{mol/g}$) ^b
Al_2O_3	–	292.1	–
2 wt% Ag/Al_2O_3	2.09	222.4	13.63
4 wt% Ag/Al_2O_3	3.45	239.8	42.67
8 wt% Ag/Al_2O_3	7.98	209.9	156.35
4 wt% Ag/Al_2O_3-L	0.53	236.4	1.77

^a Measured by ICP method.

^b Measured by H_2-O_2 titration.

below 200 nm [44]. To avoid the problem caused by the strong absorbance of Al_2O_3 , in our case, the spectrum of bare alumina was subtracted from those of $\text{Ag}/\text{Al}_2\text{O}_3$. By using such subtractive UV–vis spectra, the high extinction coefficients for $\text{Ag}_n^{\delta+}$ and Ag_n^0 clusters and the “invisibility” of some Ag^+ ions only result in an underestimate of the quantity of highly dispersed Ag^+ ions. In other words, it is really the case that isolated Ag^+ ions are predominant over $\text{Ag}/\text{Al}_2\text{O}_3$ regardless of the silver loadings. Meanwhile, keeping the extremely high UV–vis extinction coefficients for $\text{Ag}_n^{\delta+}$ and Ag_n^0

clusters in mind, it is reasonable that the two kinds of Ag clusters are “visible” in UV–vis analysis for the catalysts with 2–4 wt% Ag loadings, while they are “invisible” in XRD measurement on the same samples.

To identify the role of silver species on $\text{Ag}/\text{Al}_2\text{O}_3$ for the reduction of NO_x by methane, dilute nitric acid leaching was employed by She and Flytzani-Stephanopoulos to remove the silver particles and all weakly bound forms of silver [43]. Inspired by this, 4 wt% $\text{Ag}/\text{Al}_2\text{O}_3$ was leached with 10% HNO_3 and then calcined at the

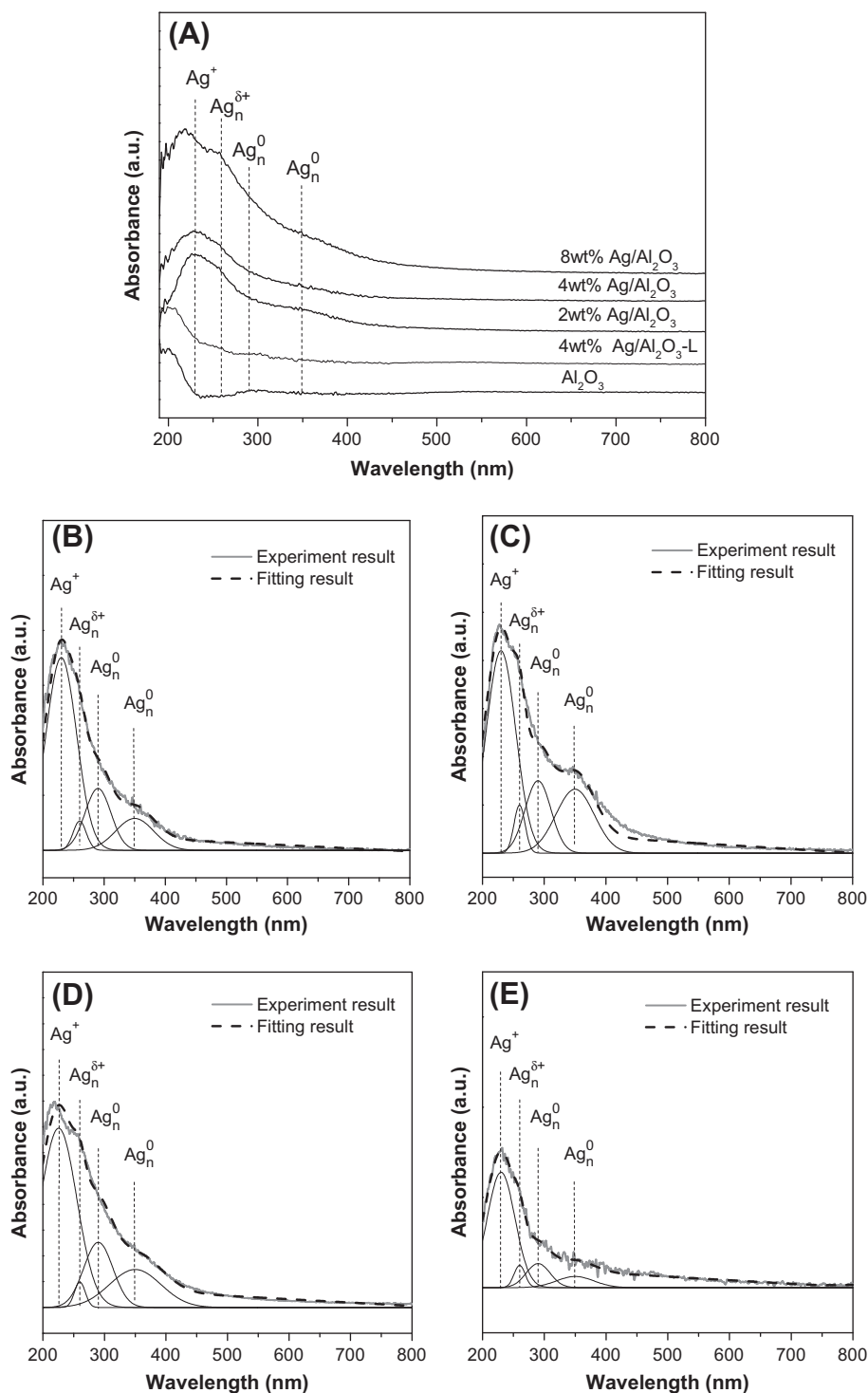


Fig. 1. UV–vis spectra of $\text{Ag}/\text{Al}_2\text{O}_3$ with different loadings (A), and deconvoluted spectra of 2 wt% $\text{Ag}/\text{Al}_2\text{O}_3$ (B), 4 wt% $\text{Ag}/\text{Al}_2\text{O}_3$ (C), 8 wt% $\text{Ag}/\text{Al}_2\text{O}_3$ (D), and 4 wt% $\text{Ag}/\text{Al}_2\text{O}_3\text{-L}$ (E).

Table 2

The percentage of different silver species calculated by analysis of the integrated peak area of the deconvoluted UV/vis spectra.

Sample	Percentage of Ag species (%)			
	Ag ⁺ (230 nm)	Ag _n ^{δ+} (260 nm)	Ag _n ⁰ (290 nm) ^a	Ag _n ⁰ (350 nm) ^b
2 wt% Ag/Al ₂ O ₃	64.65 (22.6) ^d	4.51 (10.4)	17.57 (20.8)	13.27 (30.9)
4 wt% Ag/Al ₂ O ₃	60.17 (22.9)	6.61 (10.6)	14.74 (20.4)	18.48 (30.4)
8 wt% Ag/Al ₂ O ₃	61.27 (22.8)	2.58 (10.5)	17.83 (20.6)	18.32 (30.8)
4 wt% Ag/Al ₂ O ₃ -L ^c	72.20 (22.4)	5.38 (10.0)	12.97 (20.0)	9.45 (30.2)

^a Ag_n⁰, metallic silver cluster at 290 nm.^b Ag_n⁰, metallic silver cluster at 350 nm.^c Leached by dilute nitric acid.^d Half peak width of the deconvoluted peak.

desired temperature. In good agreement with the results mentioned above [43], the silver nanoparticles were effectively removed by this pre-treatment, which was confirmed by TEM characterization (Fig. S3) and ICP measurement (Table 1). As suggested by UV–vis measurement (Fig. 1 and Table 2), meanwhile, weakly bound Ag⁺ ions on 4 wt% Ag/Al₂O₃ were also removed by this process, leaving strongly bound Ag⁺ ions on the surface of Al₂O₃.

3.2. Kinetic results of NOx reduction by ethanol on Ag/Al₂O₃ with different Ag loadings

Fig. 2A shows the Arrhenius-type plot for the reaction rate of the reduction of NOx by ethanol over Ag/Al₂O₃ with different Ag loadings. Pure alumina exhibits the lowest NOx conversion rate while silver doping greatly enhances the reaction rates. Noticeably, the leached sample of Ag/Al₂O₃-L exhibited the same NOx conversion rate as its parent sample of 4 wt% Ag/Al₂O₃, indicating that oxidized silver species, particularly strongly bound Ag⁺ ions, are the active sites responsible for the reduction of NOx by ethanol.

H₂–O₂ titration was used to evaluate the amount of accessible silver species on Ag/Al₂O₃ with different Ag loadings. As shown in Table 1, the H₂ consumption for 2 wt%, 4 wt%, 8 wt%, and 4 wt% Ag/Al₂O₃-L samples was 13.63, 42.67, 156.35, and 1.77 μmol H₂/g, respectively. These results were further used to determine the turnover frequency for NOx reduction, with results shown in Fig. 2B. 2 wt% Ag/Al₂O₃ exhibits a much higher TOF value if compared to that of 4 wt% and 8 wt% Ag/Al₂O₃, while the latter two give similar TOF values, in accordance with the ratio of oxidized silver species to metallic silver species (Table 2). This result demonstrates the superior activity of oxidized silver species for NOx reduction. Interestingly, the leached sample of 4 wt% Ag/Al₂O₃ exhibits the highest TOF value, further confirming that highly dispersed Ag⁺ ions are responsible for the reduction of NOx by ethanol.

The apparent activation energy is given in Table 3, obtained from Fig. 2A. Over pure Al₂O₃, the activation energy for the reduction of NOx by ethanol was up to 47.0 kJ/mol, while introduction of Ag obviously decreases the *E*_a values. After Ag loading, it should be noted that similar activation energies were observed in the range of 36.8–39.1 kJ/mol. This result strongly suggests that highly dispersed Ag⁺ ions play a crucial role in the reduction of NOx by ethanol, which is in good agreement with the results of She and Flytzani-Stephanopoulos [43]. Table 3 also lists the apparent activation energy for the reduction of NOx by different reductants over Ag/Al₂O₃. Obviously, the employed reductants greatly change the *E*_a values for NOx reduction over Ag/Al₂O₃. As for reduction of NOx by ethanol over 2 wt% Ag/Al₂O₃ calcined at 973 K for 15 h, an *E*_a value of 57 kJ/mol was reported by Johnson et al. [50], which is higher than that of our experimental results presented here. This difference possibly originates from differences in the catalyst preparation manner and calcination process.

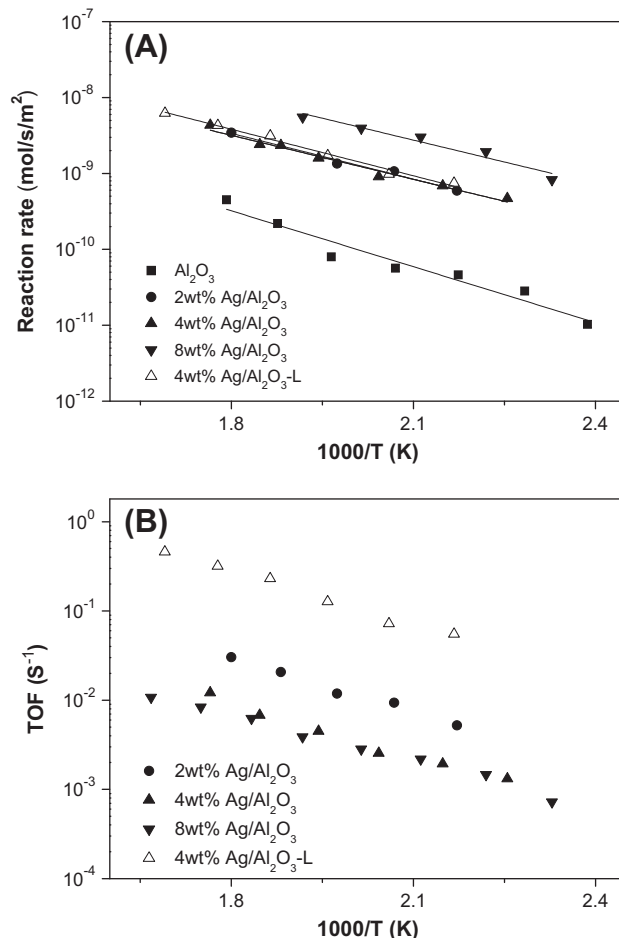


Fig. 2. (A) Reaction rates of NOx conversion to N₂ by ethanol over pure Al₂O₃ (■) and Ag/Al₂O₃ with Ag loading of 2 wt% (●), 4 wt% (▲), 8 wt% (▼), and 4 wt% Ag/Al₂O₃-L (△); (B) TOF of NOx conversion to N₂ over Ag/Al₂O₃ with Ag loading of 2 wt% (●), 4 wt% (▲), 8 wt% (▼), and 4 wt% Ag/Al₂O₃-L (△). Conditions: NO 800 ppm, C₂H₅OH 1565 ppm, O₂ 10%, H₂O 10%, N₂ balance, GHSV: 300,000 h⁻¹.

3.3. Steady state in situ DRIFTS study of the partial oxidation of ethanol on Ag/Al₂O₃ with different Ag loadings

Considering that the HC–SCR of NOx starts with the partial oxidation of the reductant, the in situ DRIFTS spectra observed during partial oxidation of ethanol over Ag/Al₂O₃ with different silver loadings were investigated first. Fig. 3A shows the in situ DRIFTS spectra of pure Al₂O₃ in a flow of C₂H₅OH (1565 ppm) + O₂ (10%) in the temperature range 473–873 K at steady state. Exposure of this sample to the feed gas resulted in the appearance of six peaks (1655, 1591, 1570, 1466, 1392, and 1335 cm⁻¹) within the wave

Table 3
Apparent activation energies of NO_x reduction by different reductants over Ag/Al₂O₃.

Sample	Activation energy (kJ/mol)	Reductant	Refs.
Al ₂ O ₃ ^a	47.0	C ₂ H ₅ OH	This work
2 wt% Ag/Al ₂ O ₃ ^a	38.5	C ₂ H ₅ OH	This work
4 wt% Ag/Al ₂ O ₃ ^a	37.0	C ₂ H ₅ OH	This work
8 wt% Ag/Al ₂ O ₃ ^a	39.1	C ₂ H ₅ OH	This work
4 wt% Ag/Al ₂ O ₃ -L ^b	36.8	C ₂ H ₅ OH	This work
2 wt% Ag/Al ₂ O ₃ ^c	57	C ₂ H ₅ OH	[50]
4 wt% Ag/Al ₂ O ₃ -L	94.7	CH ₄	[43]
2 wt% Ag/Al ₂ O ₃	61	C ₃ H ₈ + H ₂	[41]
2 wt% Ag/Al ₂ O ₃	67	C ₆ H ₁₄	[51]

^a Calcined at 873 K for 3 h.

^b Leached by dilute nitric acid and then calcined at 723 K and 873 K for 3 h.

^c Calcined at 973 K for 15 h.

number range 2300–1200 cm⁻¹. Peaks at 1570 and 1466 cm⁻¹ were assigned to $\nu_{as}(\text{OCO})$ and $\nu_s(\text{OCO})$ of acetate, respectively [45,51,52]. It should be noted that the other peaks located at 1655, 1591, 1392, and 1335 cm⁻¹ decreased simultaneously and gradually in their intensity with rising temperature and disappeared at the same temperature of 773 K. This result indicates that the four peaks may be due to the same species derived from the partial oxidation of ethanol on Al₂O₃, and their assignments will be discussed below.

The same experiments were performed on Ag/Al₂O₃ with different Ag loadings. The DRIFTS spectra of adsorbed species on 2 wt% Ag/Al₂O₃ in flowing C₂H₅OH + O₂ at different temperatures are shown in Fig. 3B. Similar to the spectra of pure Al₂O₃ (Fig. 3A), peaks at 1578 and 1464 cm⁻¹ were also assigned to acetate, while new peaks at 1633 and 1416 cm⁻¹ were observed over the whole temperature range. According to our earlier studies [5,27–29,32,34,53], the two peaks at 1633 and 1416 cm⁻¹ together with the peak at 1336 cm⁻¹ were assigned to the asymmetric stretching vibration, symmetric stretching vibration, and C–H deformation vibration modes of an adsorbed enolic species, respectively. Meanwhile, the peaks at 1591 and 1392 cm⁻¹ were also detected, whereas the peak at 1655 cm⁻¹ was not observed, possibly masked by the strong peak at 1633 cm⁻¹.

Further increasing the Ag loading to 4 wt% (Fig. 3C), stronger peaks at 1633 and 1416 cm⁻¹ were observed compared with those of 2 wt% Ag/Al₂O₃ (Fig. 3B). Actually, within the wide temperature region 473–723 K, the intensity of the peak at 1633 cm⁻¹ was the highest in Fig. 3C. This result strongly suggests that large amounts of enolic species were formed during the partial oxidation of ethanol on 4 wt% Ag/Al₂O₃. The acetate peaks at 1570 and 1470–1466 cm⁻¹ were also observed; however, their intensity was much lower than that of enolic species within the temperature range of 473–723 K. In addition, a shoulder at 1392 cm⁻¹ was observed at 473 K, and its intensity gradually decreased with rising temperature.

When the Ag loading increased to 8 wt% (Fig. 3D), the enolic species peak at 1637 cm⁻¹ was still the strongest within the temperature range 473–673 K. The acetate peaks were observed at 1574 and 1460 cm⁻¹ over the whole temperature region and became dominant at 723 K, at which point the enolic species peaks were hardly observed. As for 4 wt% Ag/Al₂O₃ at the same temperature of 723 K (Fig. 3C), however, the enolic species peaks were much stronger than those of acetate. These results indicated that at high temperatures, the increase of Ag loading from 4 wt% to 8 wt% was favorable for acetate formation at the expense of the enolic species formation during the partial oxidation of ethanol.

The same experiments were also carried out on the leached sample of 4 wt% Ag/Al₂O₃-L, with the result shown in Fig. 3E. The appearance of peaks at 1633, 1412, and 1336 cm⁻¹ suggests the formation of enolic species. Compared with the parent sample of

4 wt% Ag/Al₂O₃ (Fig. 3C), the intensity of enolic species peaks decreased obviously, while the acetate peaks (1575 and 1466 cm⁻¹) became dominant over the whole temperature region.

As described above, a new species was formed during the partial oxidation of ethanol over pure Al₂O₃. Thus, DFT calculations were carried out to investigate the structure of this species adsorbed on the pure Al₂O₃ surface. Different models were designed for simulation of its structure and FTIR spectrum, which involved the length of carbon chain, the structure of the catalyst, and the interaction of the adsorbed species with the catalyst surface. We found that the peaks at 1655, 1591, 1392, and 1335 cm⁻¹ can be assigned to an enolic species (CH₂=CH–CH=CH–O–Al₆O₅(OH)₈), which only interacts with Al sites (thereafter denoted as RCH=CH–O–Al), as shown in the insert of Fig. 4. Apparently, the calculated FTIR spectrum (Fig. 4) is of reasonable similarity to the corresponding experimental one (Fig. 3A). The asymmetric stretching vibration mode of the enolic species, mainly involved in the stretching vibration of the C=C–C=O structure, was calculated at 1634 cm⁻¹, which is 21 cm⁻¹ lower than the experimental harmonic frequency (1655 cm⁻¹). Compared to the experimental value, the calculated symmetric stretching vibrational mode of this species agreed within less than 6 cm⁻¹ (1591 cm⁻¹ against 1597 cm⁻¹), and this case mainly concerns the stretching vibration of the C=C–C=C chain while the vibration of the C–O bond has hardly any contribution. The calculated C–H deformation vibration modes (1406 and 1324 cm⁻¹) were also close to the experimental results (1392 and 1335 cm⁻¹). Obviously, there is excellent agreement between the calculated vibration spectrum and the experimental one, supporting our assignment of surface enolic species adsorbed only on Al sites (RCH=CH–O–Al).

Furthermore, a similar feature was observed when exposing Al₂O₃ to 2,3-dihydrofuran (C₄H₆O), which contains a ring C–C=C–O structure. As shown in Fig. 5, the peaks at 1660, 1605, 1392, and 1315 cm⁻¹ are due to this structure adsorbed on the Al₂O₃ surface. This result further confirms our assignments concerning the surface enolic species adsorbed on Al sites. In addition, the peaks at 1574 and 1458 cm⁻¹ appearing in Fig. 5 were attributed to surface acetate, indicating a transformation of the enolic species adsorbed on Al₂O₃.

In our earlier study [28,53], the characteristic frequencies of enolic species adsorbed on the Ag/Al₂O₃ surface (1633, 1416, and 1336 cm⁻¹) were identified by DFT calculations (Fig. 6). DFT calculations also showed that this enolic species would be present in the form of CH₂=CH–O–Ag (thereafter denoted as RCH=CH–O–Ag) and/or CH₂=CH–CH=CH–O–Al–Ag (thereafter denoted as RCH=CH–O–Al–Ag). In both models, silver participated in the formation of adsorbed enolic species, indicating that the enolic species over Ag/Al₂O₃ surface are prone to adsorb on or close to Ag sites, which exhibits an intimate contact with the active phase.

3.4. Dynamic study of the formation of –NCO on Ag/Al₂O₃ with different Ag loadings

It has been widely accepted that –NCO species is a vital intermediate for the SCR of NO_x by ethanol and other hydrocarbons; thus, much attention has focused on its formation and reactivity [13,46,54–61]. With this in mind, the relationship between –NCO formation and the consumption of enolic species and acetate was investigated on pure Al₂O₃ and Ag/Al₂O₃. The reactivity of enolic species and acetate, formed during the C₂H₅OH + O₂ reaction on pure Al₂O₃ at 673 K, toward NO + O₂ was evaluated by the transient response of the DRIFTS method (Fig. 7A). After the catalyst was exposed to C₂H₅OH + O₂ for 60 min, strong peaks (1655, 1591, 1392, and 1335 cm⁻¹) due to enolic species interaction with Al sites were observed, along with the formation of acetate (1570 and 1466 cm⁻¹). Switching the feed gas to NO + O₂ resulted in

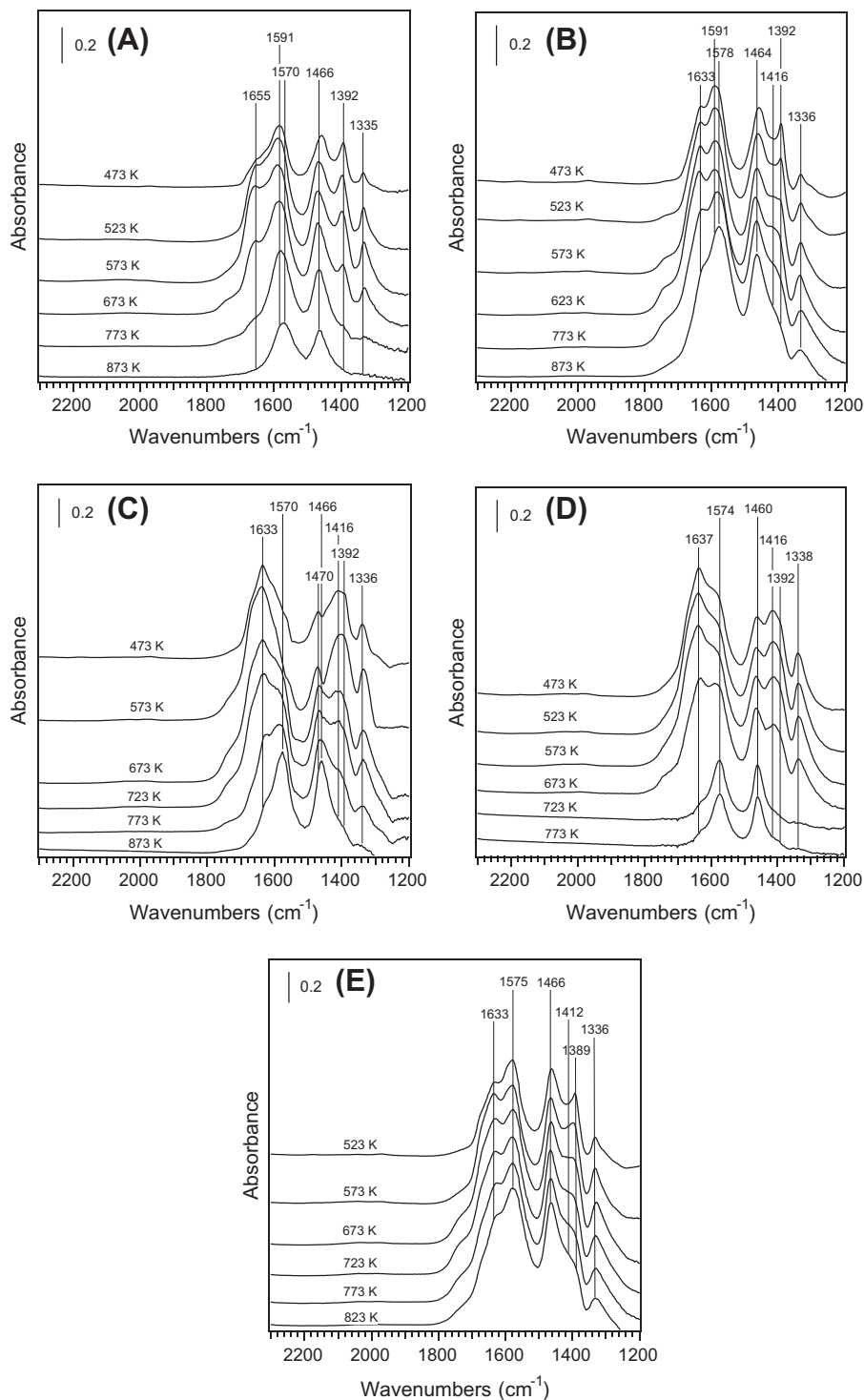


Fig. 3. In situ DRIFTS spectra of adsorbed species on Al_2O_3 (A), $\text{Ag}/\text{Al}_2\text{O}_3$ with Ag loading of 2 wt% (B), 4 wt% (C), and 8 wt% (D), and 4 wt% $\text{Ag}/\text{Al}_2\text{O}_3\text{-L}$ (E) in steady states in a flow of $\text{C}_2\text{H}_5\text{OH} + \text{O}_2$ at different temperatures. Conditions: $\text{C}_2\text{H}_5\text{OH}$ 1565 ppm, O_2 10%, N_2 balance.

the appearance of peaks at 2253 and 2233 cm^{-1} . Many studies have been devoted to the assignment of these two peaks, which have been attributable to $-\text{NCO}$ bound on octahedrally coordinated Al^{VI} ions ($\text{Al}^{\text{VI}}-\text{NCO}$) and on tetrahedrally coordinated Al^{IV} sites ($\text{Al}^{\text{IV}}-\text{NCO}$), respectively [56–60]. In order to clearly observe the quantitative changes in the surface species mentioned above, the spectra in the range of 1200–2300 cm^{-1} were converted into Kubelka–Munk function [62] and fitted on the basis of the deconvoluted curves (see Supplementary information and Fig. S4). After

Kubelka–Munk conversion, the integrated areas of peaks at 1655, 1466, 2233, and 2253 cm^{-1} in Fig. 7A are displayed as a function of time on stream as shown in Fig. 7B. Switching the feed gas to $\text{NO} + \text{O}_2$ resulted in a significant decrease in the intensity of peaks due to enolic species, while the decrease in the intensity of acetate peaks is much slower than that of enolic species on the same time scale. Meanwhile, this decrease was accompanied by the appearance of the peaks due to $-\text{NCO}$, whose intensity increased with time on stream, reaching a maximum at 5 min and then decreasing

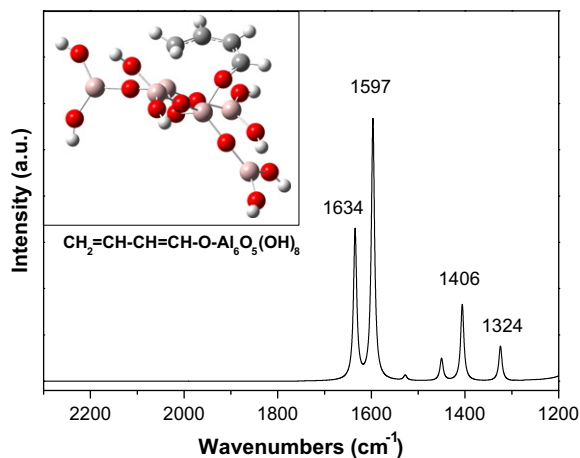


Fig. 4. Molecular structure of the calculational model for the surface enolic species on Al_2O_3 (inset figure) and its calculated FTIR spectrum.

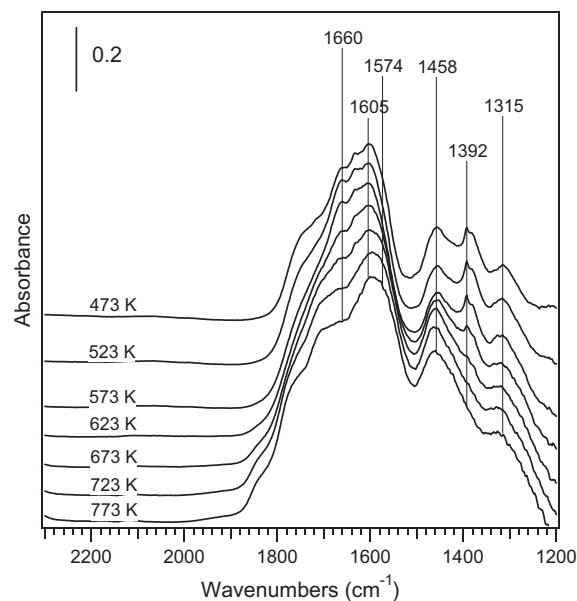


Fig. 5. In situ DRIFTS spectra of Al_2O_3 in the steady states at different temperatures in a flow of 2,3-dihydrofuran + N_2 .

gradually. These results confirm that the enolic species bound on Al sites is more active toward $\text{NO} + \text{O}_2$ to form $-\text{NCO}$ than is acetate at this temperature. In addition, the appearance of peaks at 1302 and 1583 cm^{-1} indicates the formation of surface nitrate species [14,15,28]. The same set of experiments was also performed on pure Al_2O_3 at 863 K, at which point the NO_x conversion reached a maximum (result not shown here). In this case, only acetate was observed after exposure to $\text{C}_2\text{H}_5\text{OH} + \text{O}_2$. Switching the feed gas to $\text{NO} + \text{O}_2$ resulted in a quick decrease in the intensity of acetate peaks, which was accompanied by the formation of $\text{Al}-\text{NCO}$.

The reactivity of the partial oxidation products of ethanol on 4 wt% $\text{Ag}/\text{Al}_2\text{O}_3$ has been evaluated in essentially the same manner as above (Fig. 7C and D). After exposure to $\text{C}_2\text{H}_5\text{OH} + \text{O}_2$ at 673 K for 60 min, the enolic species bound on or close to Ag sites exhibited strong peaks at 1635, 1419, and 1338 cm^{-1} , while the characteristic vibration modes of the enolic species adsorbed on Al sites were hardly observed. Strong peaks assignable to acetate were observed at 1578 and 1464 cm^{-1} . After switching the feed gas to $\text{NO} + \text{O}_2$, the peaks due to enolic species intimately linked to Ag

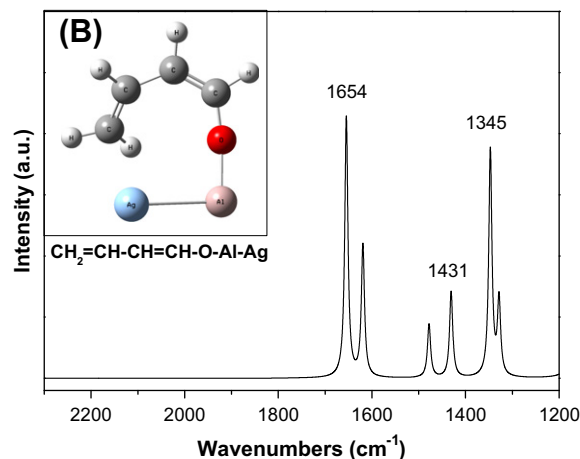
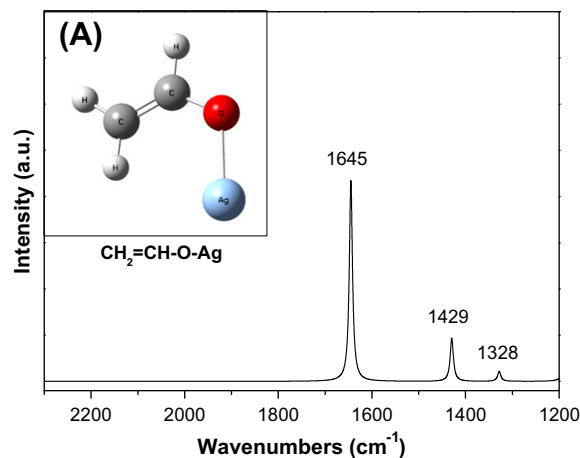


Fig. 6. Molecular structures of the calculational models of $\text{CH}_2=\text{CH}-\text{O}-\text{Ag}$ (A) and $\text{CH}_2=\text{CH}-\text{CH}=\text{CH}-\text{O}-\text{Al}-\text{Ag}$ (B) for the surface enolic species adsorbed on or close to Ag sites of $\text{Ag}/\text{Al}_2\text{O}_3$ (inset figure) and their calculated FTIR spectra.

sites decreased quickly, whereas the concentration of surface acetate only decreased slightly on the same time scale. Simultaneously, purging with $\text{NO} + \text{O}_2$ results in the formation of $-\text{NCO}$ at 1 min, reaching a maximum at 3 min, and then decreasing gradually.

Simultaneously, the composition of the outlet gas from the in situ IR chamber was continuously monitored with a mass spectrometer, with the results shown in Fig. 7E and Fig. S5A. The final product of N_2 originating from the reaction between surface enolic species and $\text{NO} + \text{O}_2$ was calculated based on the signals of N_2 ($m/e = 28$) after clarifying the contribution of CO to $m/e = 28$. The N_2 signal in the mass spectra clearly shows that the yield of N_2 reaches its peak at essentially the same time of 3 min. Meanwhile, the mass signal of CO_2 also exhibits similar behavior with time on stream. The total amounts of N_2 and CO_2 production for 25 min were estimated by integrating the areas peaks corresponding to these two products as shown in Fig. 7E, giving the values of 204.5 and $600.6\text{ }\mu\text{mol/g-cat}$, respectively. The amounts of CO_2 and CO were further used to estimate the surface enolic species participating in the reaction. With the structural features of surface enolic species ($\text{CH}_2=\text{CH}-\text{O}-\text{Ag}$ and $\text{CH}_2=\text{CH}-\text{CH}=\text{CH}-\text{O}-\text{Al}-\text{Ag}$) in mind, its consumption was estimated to $283.1\text{--}566.2\text{ }\mu\text{mol/g-cat}$, which is fairly close to that of the final product of N_2 , $204.5\text{ }\mu\text{mol/g-cat}$. These results quantitatively confirm that the enolic species in intimate contact with the active phase plays a crucial role in the reduction of NO_x by ethanol. Over this catalyst, meanwhile, H_2-O_2 titration showed that the accessible amount of silver sites

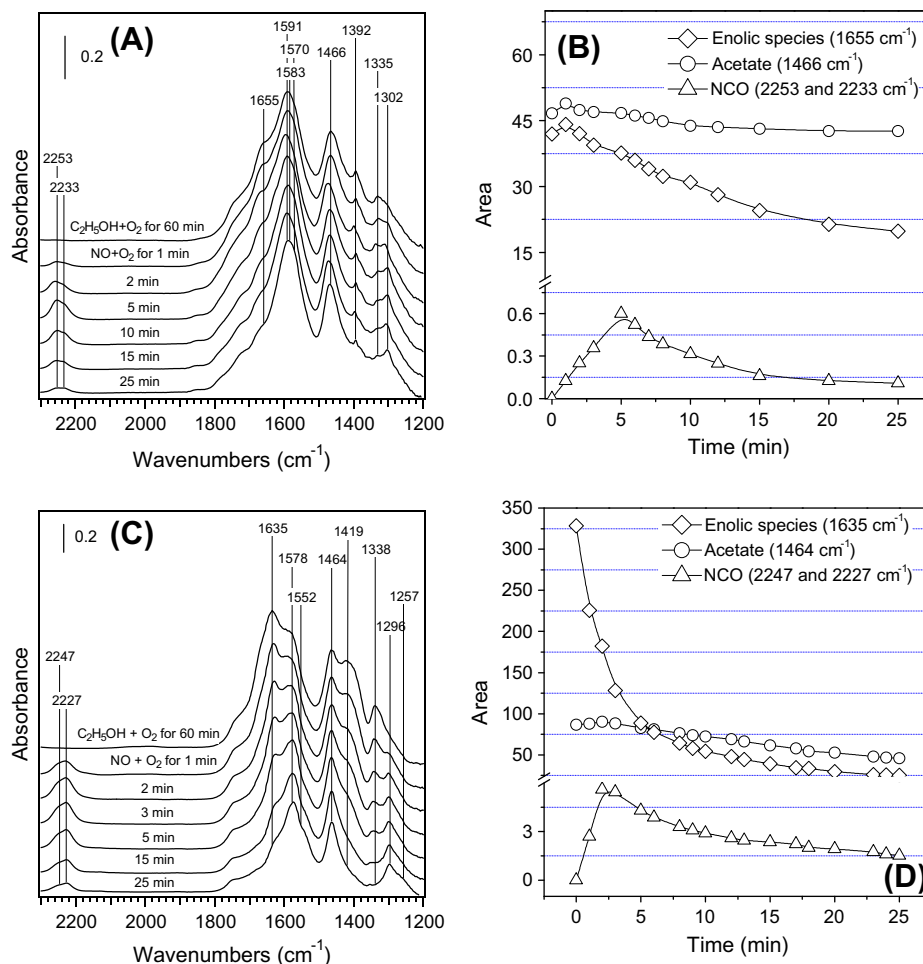


Fig. 7. Dynamic changes in situ DRIFTS spectra over Al_2O_3 (A), 4 wt% $\text{Ag}/\text{Al}_2\text{O}_3$ (C), and 4 wt% $\text{Ag}/\text{Al}_2\text{O}_3\text{-L}$ (F) as a function of time in a flow of $\text{NO} + \text{O}_2$ at 673 K. Before measurement, the catalyst was pre-exposed to a flow of $\text{C}_2\text{H}_5\text{OH} + \text{O}_2$ for 60 min at 673 K. Conditions: NO 800 ppm, $\text{C}_2\text{H}_5\text{OH}$ 1565 ppm, O_2 10%, N_2 balance (Ar balance for the case of (C) and (F)). (B), (D), and (G): time dependence of the integrated areas of the peaks of enolic species (\diamond), acetate (\circ), and $-\text{NCO}$ (Δ) for the cases of (A), (C), and (F), respectively. (E) and (H): time dependence of N_2 and CO_2 concentration calculated from the mass signals for the cases of (C) and (F), respectively.

was $85.34 \mu\text{mol}/\text{g-cat}$, which is lower than that of surface enolic species. This result indicates that not only the Ag sites, but also Al sites closely linked to Ag participate in the formation of surface enolic species, further confirming our assignment for this species.

The in situ DRIFTS combined with MS analysis was further performed on the leached sample of 4 wt% $\text{Ag}/\text{Al}_2\text{O}_3\text{-L}$. Similar to its parent sample, a sharp decrease in the intensity of peaks due to the enolic species bound on or closed to Ag sites was also observed after switching the feed gas to $\text{NO} + \text{O}_2$, while the concentration of acetate only decreased slightly (Fig. 7F and G). Meanwhile, the consumption of enolic species results in the formation of $-\text{NCO}$ at 1 min, exhibiting the maximum at 4 min, and then decreasing gradually. Based on the MS result (Fig. S5B and Fig. 7H), the consumption of enolic species over the leached sample was estimated to $65.4\text{--}130.8 \mu\text{mol}/\text{g-cat}$, as many as 23% of the value over the parent sample. As shown in Table 1, the Ag content on the former (0.53%) was about 15% of the latter's (3.45%), which is fairly close to the ratio of enolic species participating in the reaction over the two samples, confirming a relationship between the amount of enolic species and the number of Ag sites. MS analysis also showed that the produced N_2 was $45.8 \mu\text{mol}/\text{g-cat}$ over the leached sample, which is very close to the consumption of enolic species.

The enolic species intimately linked to Ag sites has higher reactivity with $\text{NO} + \text{O}_2$ than does acetate; thus, it plays a crucial role in the formation of $-\text{NCO}$ and its further reaction to produce N_2 , and is responsible for the reduction of NOx by ethanol over $\text{Ag}/\text{Al}_2\text{O}_3$. By

comparison with Fig. 7B, it can be easily seen that the enolic species intimately linked to Ag sites is more active than that adsorbed on Al sites, because the former exhibits a sharper decrease in its peak intensity than that of the latter when it reacts with $\text{NO} + \text{O}_2$. In addition, the appearance of peaks at 1257 and 1296 cm^{-1} indicates the formation of surface nitrate species [14,15,28].

Under the same conditions as those of previous experiment, we also analyzed the reactivity of enolic species and acetate when NO was introduced on 4 wt% $\text{Ag}/\text{Al}_2\text{O}_3$. The observation (Fig. S6) showed that a gradual consumption of the enolic species intimately linked with Ag sites resulted in the formation of $-\text{NCO}$, reaching the maximum at around 35 min, and then remaining constant with time. However, the consumption of enolic species and the formation of $-\text{NCO}$ were much slower than those in the presence of O_2 (Fig. 7C and D). The above results indicate that O_2 plays a crucial role in the acceleration of the reaction between enolic species and NO to form $-\text{NCO}$. These results also indicate that the $-\text{NCO}$ exhibits low reactivity toward NO in the absence of O_2 , which is in agreement with the observation of Bion et al. [56].

3.5. Steady state in situ DRIFTS study of the SCR of NOx by ethanol on $\text{Ag}/\text{Al}_2\text{O}_3$ with different Ag loadings

Fig. 8A shows the DRIFTS spectra of pure Al_2O_3 during the $\text{NO} + \text{C}_2\text{H}_5\text{OH} + \text{O}_2$ reaction at various temperatures (473–823 K) at steady state. Surface species, such as enolic species interacting

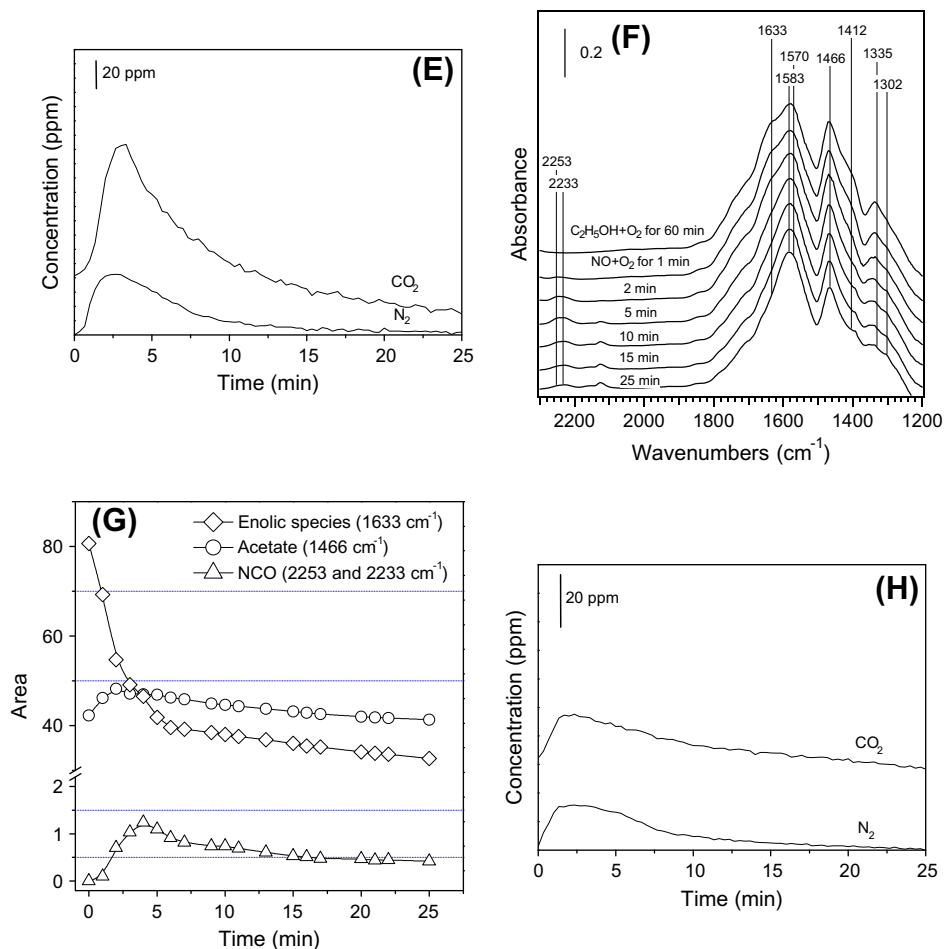


Fig. 7 (continued)

with Al sites (1655 , 1591 , 1392 and 1335 cm^{-1}), acetate (1570 and 1466 cm^{-1}), and bidentate nitrate (1583 and 1302 cm^{-1}), were observed. The Al–NCO peak located at 2253 cm^{-1} was detected in the temperature range of 623 – 873 K . However, it should be noted that its intensity was very low though large amounts of nitrate, enolic species, and acetate co-existed on the surface of Al_2O_3 .

The same set experiments was performed on $\text{Ag}/\text{Al}_2\text{O}_3$ with different Ag loadings. Fig. 8B shows the DRIFTS spectra of adsorbed species during the $\text{NO} + \text{C}_2\text{H}_5\text{OH} + \text{O}_2$ reaction over 2 wt% $\text{Ag}/\text{Al}_2\text{O}_3$ within the temperature range of 473 – 873 K at steady state. Enolic species in intimate contact with Ag sites (1633 , 1416 , and 1336 cm^{-1}), acetate (1576 and 1466 cm^{-1}), and bidentate nitrate (1587 and 1304 cm^{-1}) were clearly observed, while the enolic species adsorbed on Al sites exhibited a very weak peak at 1392 cm^{-1} . A weak peak at 2125 cm^{-1} due to $-\text{CN}$ was observed at temperatures above 623 K , giving an increased intensity with rising temperature [4]. It should be noted that a strong peak attributable to $-\text{NCO}$ (2231 cm^{-1}) was detected within the temperature region 623 – 873 K , which was accompanied by a shoulder at 2253 cm^{-1} , especially at low temperatures.

The characteristic peaks of $-\text{NCO}$ located around 2230 and 2250 – 2260 cm^{-1} have been commonly observed on $\text{Ag}/\text{Al}_2\text{O}_3$ during HC–SCR, while the assignments of their coordination sites are still controversial. Bion et al. [56,57] and Thibault-Starzyk et al. [58] observed the characteristic frequencies of $-\text{NCO}$ on $\text{Ag}/\text{Al}_2\text{O}_3$ located at 2255 – 2265 and 2228 – 2240 cm^{-1} , which were assigned to $-\text{NCO}$ species coordinated with octahedral Al^{3+} ions ($\text{Al}^{\text{VI}}-\text{NCO}$) and tetrahedral Al^{3+} sites ($\text{Al}^{\text{IV}}-\text{NCO}$), respectively. During the reduction of NO_x by ethanol and propene on $\text{Ag}/\text{Al}_2\text{O}_3$, the two

peaks at 2258 – 2262 and 2230 – 2235 cm^{-1} were detected by Ukisu et al. [63], Kameoka et al. [14,55], and Sumiya et al. [13,64]. The high-frequency peak was assigned to Al–NCO, while the low-frequency one was attributed to adsorption on Ag sites (Ag–NCO). To identify the adsorption sites of $-\text{NCO}$ on the $\text{Ag}/\text{Al}_2\text{O}_3$ surface, DFT calculations have been performed by Gao and He [61]. The Al–NCO group exhibits a calculated vibrational frequency at 2267 cm^{-1} , which is an excellent agreement with the experimental value (around 2260 cm^{-1}). The calculated mode of $(\text{OH})_2\text{Al}-\text{O}-\text{Ag}-\text{NCO}$ shows the asymmetric stretching frequency of $-\text{NCO}$ at 2215 cm^{-1} , also close to the corresponding experimental one (around 2230 cm^{-1}), indicating that the low-frequency peak may contribute to the $-\text{NCO}$ species adsorbed on or close to Ag sites. By using an elegant short time on stream in situ spectroscopic transient isotope experimental technique, more recently, Chansai et al. [46,65] proposed that there may be two types of $-\text{NCO}$ species during the reduction of NO_x by hydrocarbons over $\text{Ag}/\text{Al}_2\text{O}_3$. One is a slowly reacting spectator $-\text{NCO}$ species, probably adsorbed on the oxide support of Al_2O_3 , while another is related to reactive $-\text{NCO}$, possibly on or close to the active silver phase. With this in mind, herein, the peak at around 2230 cm^{-1} appearing in Fig. 8B is tentatively assigned to the $-\text{NCO}$ bound on and/or close to Ag sites (hereafter noted as Ag–NCO), while the peak at around 2250 cm^{-1} is speculatively attributed to $-\text{NCO}$ species bound to Al (hereafter noted as Al–NCO).

During the reduction of NO_x by ethanol on 4 wt% $\text{Ag}/\text{Al}_2\text{O}_3$ (Fig. 8C), bidentate nitrate (1583 and 1302 cm^{-1}), bridging nitrate (1612 cm^{-1}), acetate (1572 , 1466 cm^{-1}), and $-\text{CN}$ (2125 cm^{-1}) were observed [8,14,15]. It is worthwhile to note that the peak at

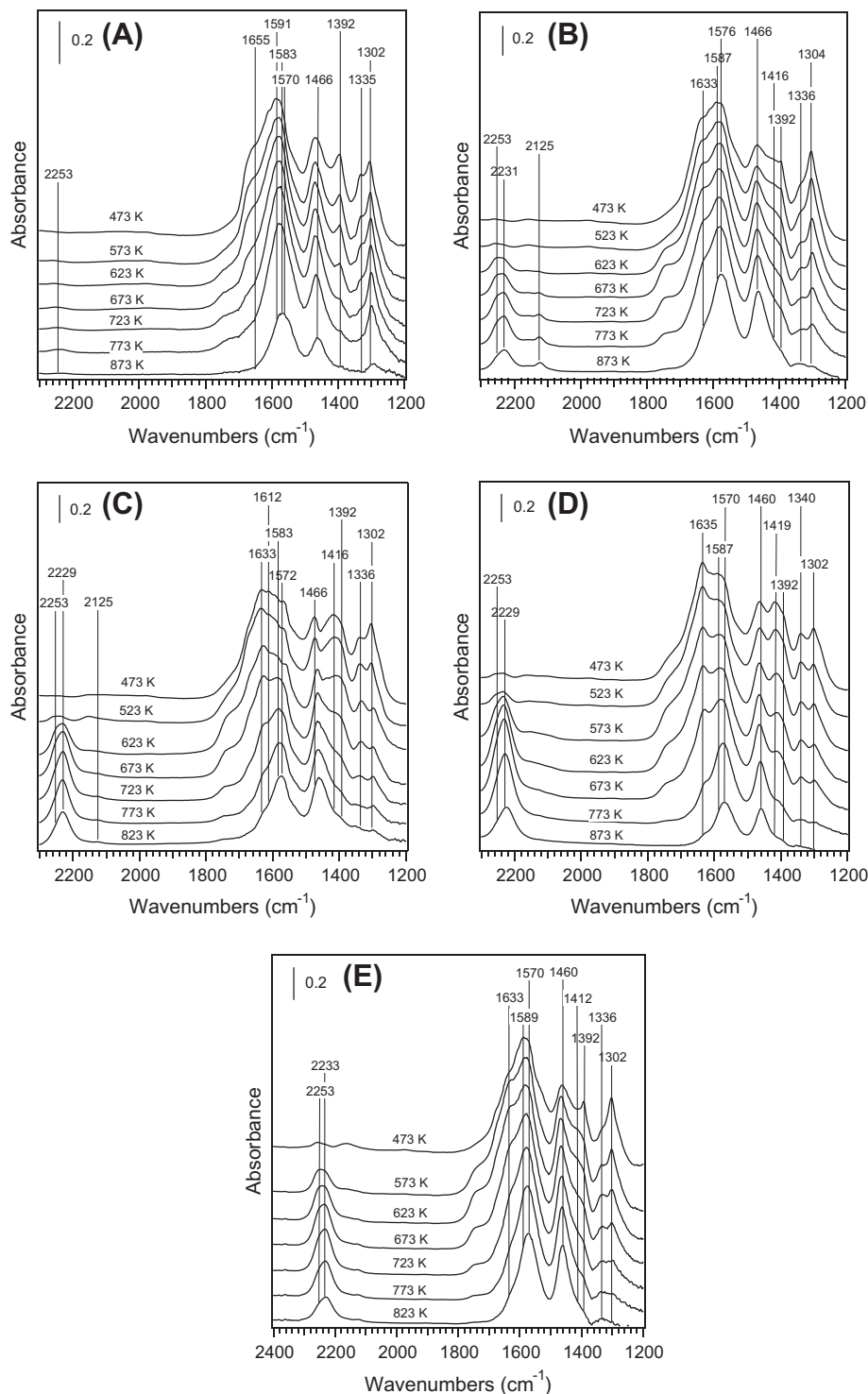


Fig. 8. In situ DRIFTS spectra of adsorbed species in steady states on Al_2O_3 (A), $\text{Ag}/\text{Al}_2\text{O}_3$ with Ag loading of 2 wt% (B), 4 wt% (C), 8 wt% (D), and 4 wt% $\text{Ag}/\text{Al}_2\text{O}_3\text{-L}$ (E) in a flow of $\text{C}_2\text{H}_5\text{OH} + \text{NO} + \text{O}_2$ at different temperatures. Conditions: NO 800 ppm, $\text{C}_2\text{H}_5\text{OH}$ 1565 ppm, O_2 10%, N_2 balance.

1633 cm^{-1} assignable to the enolic species intimately linked with Ag sites is the strongest within the low temperature range of 473–673 K, which is similar to that of the partial oxidation of ethanol on the same catalyst (Fig. 3C). In comparison with Fig. 8B, the intensity of Ag–NCO peak at (2229 cm^{-1}) is much higher, while the shoulder due to Al–NCO (2253 cm^{-1}) is lower. These results clearly show that an increase in Ag loading enhances the formation of the enolic species bound on and/or close to Ag sites, and its further transformation to the key intermediate of Ag–NCO, finally

accounting for the key role of Ag in NO_x reduction. We also measured the in situ DRIFTS spectra of 8 wt% $\text{Ag}/\text{Al}_2\text{O}_3$ during the reduction of NO_x by ethanol (Fig. 8D), which shows much more strongly the enolic species and –NCO both intimately linked with silver sites at temperatures below 573 K, indicating a higher NO_x conversion rate if compared with the results for 4 wt% $\text{Ag}/\text{Al}_2\text{O}_3$. Within the temperature range 573–873 K, meanwhile, the appearance of a much stronger Ag–NCO peak at 2229 cm^{-1} along with a

much lower Al–NCO characteristic vibration confirms the crucial role of Ag in the formation of this species.

The same set of experiment was also performed on the leached sample of 4 wt% Ag/Al₂O₃ (Fig. 8E). The appearance of peaks at 1633, 1412, and 1336 cm⁻¹ indicates the formation of enolic species intimately linked to Ag sites. However, the enolic species peaks exhibit much lower intensity if compared with those on the parent sample (Fig. 8C), deriving from the lower Ag content in the leached sample. –NCO species, as another intermediate linked to Ag sites, also shows a decreased intensity. Meanwhile, the peaks due to acetate and nitrates were observed while their intensity has no big difference if compared with Fig. 8C.

3.6. Influence of water vapor and CO₂ on the SCR of NO_x by ethanol on Ag/Al₂O₃

Water vapor and CO₂ are commonly presented in diesel engine exhaust, and the presence of which has a great influence on the reaction pathway of the HC–SCR [4,23,56]. In our previous work [5], in situ DRIFTS results showed that the presence of water vapor promoted the formation of enolic species intimately linked to Ag sites, while suppressed the formation of acetate species. These opposite effects of water vapor on the two species may drive from their different behaviors in the adsorbed sites, identification of which may provide important implications for understanding water vapor effect on the HC–SCR. In this study, meanwhile, in situ DRIFTS method was further used to study the impact of the co-existence of water vapor and CO₂ on the partial oxidation of ethanol and on the NO_x reduction on 4 wt% Ag/Al₂O₃ (see Supplementary information and Fig. S7). Compared with Figs. 3C and 7C, it was found that the presence of both hardly changed the formation and reactivity of enolic species bound on or close to silver sites, indicating its key role under practical conditions.

3.7. Influence of Ag loading on the acid–base property of Al₂O₃

Considering that the acid–base property is a fundamental aspect of the activity of alumina-supported catalysts, NH₃ adsorption was performed on pure Al₂O₃ and 4 wt% Ag/Al₂O₃, respectively [66,67]. These results (see Supplementary information, Figs. S8 and S9) indicate that the loading of Ag on Al₂O₃ increases the Lewis acidity while decreases the Brønsted acidity. These changes may

modify the behavior of adsorbed species such as enolic species, acetate, and –NCO species, and thus changing the reaction pathway of HC–SCR and the activity of employed catalysts. A clear picture of the relationship between the acid–base properties of our catalysts and their activity can be expected in the near future.

4. Discussion

It was apparent that the enolic species adsorbed on Al sites (RCH=CH–O–Al) was formed during the partial oxidation on pure Al₂O₃, which was accompanied by the formation of acetate. During the partial oxidation of ethanol over 2 wt% Ag/Al₂O₃, the enolic species bound on or close to silver sites, present as RCH=CH–O–Ag and RCH=CH–O–Al–Ag, was clearly observed. Further increase of the Ag loading to 4 wt% increases the intensity of such enolic species, while the enolic species bound on Al sites are hardly observed. Considering that the molar ratio of Al/Ag on 4 wt% Ag/Al₂O₃ was as much as 60, this result strongly suggests that the addition of Ag significantly enhances the formation of the enolic species, which is preferably adsorbed on or close to silver sites, exhibiting an intimate contact with the active phase. When the Ag loading increased to 8 wt%, such enolic species intimately linked to the active phase was still dominant in the temperature range 473–673 K. On all Ag/Al₂O₃ samples, UV–vis analysis (Fig. 1 and Table 2) shows that Ag species are mainly present in the oxidized state (Ag⁺ and Ag_n^{δ+}) [40–45]. Our kinetic measurements confirm that such silver species, particularly strongly bound Ag⁺ ions, are the active sites responsible for the reduction of NO_x by ethanol. Thus, we propose that the enolic species on Ag/Al₂O₃ surface possibly adsorb on or close to isolated Ag⁺ ions and/or Ag_n^{δ+} clusters, as shown in Fig. 9. This enolic species was clearly observed on the leached sample, in which Ag⁺ ions were predominant, supporting our assumption. This assignment was also confirmed by the higher amount of surface enolic species than the amount of accessible silver sites on 4 wt% Ag/Al₂O₃.

During the partial oxidation of ethanol on all samples, meanwhile, the peaks due to surface acetate were clearly observed, with the same characteristic vibrational frequencies (1570–1578, 1460–1468 cm⁻¹) regardless of silver loadings. The same situation also occurred for the SCR of NO_x by ethanol (Fig. 8). These results indicate that the acetate species formed during the partial oxidation of

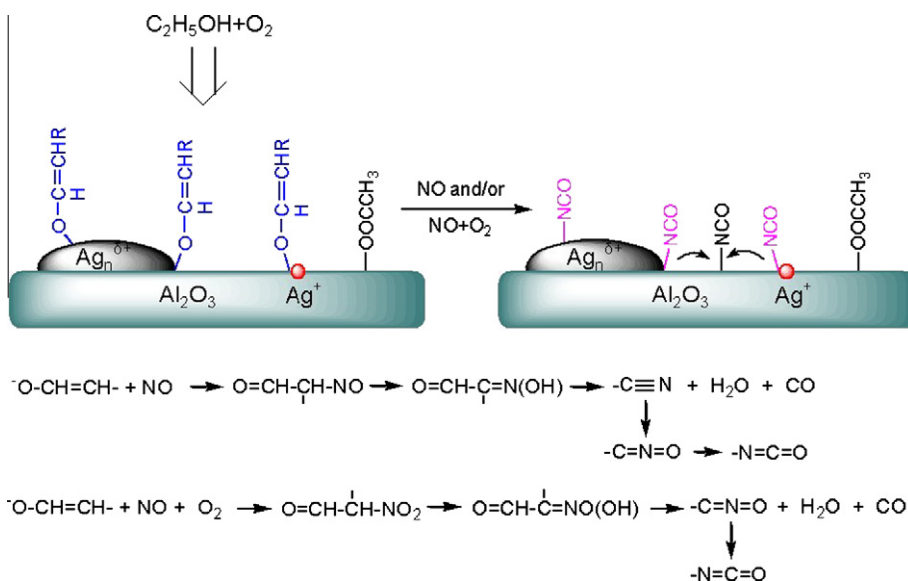


Fig. 9. Schematic models of enolic species and –NCO formation on Ag/Al₂O₃.

ethanol may mainly adsorb on Al sites instead of Ag sites. The adsorption characteristics of acetate on the surface of Ag/Al₂O₃ catalyst have been investigated by DFT calculations and DRIFTS [68]. The calculated vibrational spectrum of acetate adsorbed on Al sites, present as CH₃COO–Al₂O(OH)₂, is in good agreement with the experimental one, while there is a large error between the calculated and experimental vibrational modes of the acetate species bound on silver sites, further confirming that acetate species over Ag/Al₂O₃ are prone to interact with Al sites, as shown in Fig. 9.

Such different features in the adsorption sites for the enolic and acetate species on Ag/Al₂O₃ may contribute to their different reactivity toward NO + O₂ (and/or NO), and their role in the formation of –NCO during the reduction of NO_x by ethanol. Specifically, the surface enolic species adsorbed on or close to Ag sites possesses much higher activity in reaction with NO + O₂ and/or NO to form Ag–NCO species than enolic species and acetate bound on Al sites. A combined mass measurement further shows that the consumption of enolic species is fairly close to the formation of the final product N₂ over both 4 wt% Ag/Al₂O₃ and the leached sample. These results demonstrate the crucial role of enolic species intimately linked with Ag sites in the SCR of NO_x by ethanol.

In organic synthesis, enols, and/or enolate anions were common intermediates in nitrosation reaction between aldehydes/ketones and the substrates containing NO group such as HONO, NO⁺, NO[–], neutral NO, C(NO₂)₄, and [Fe(CN)₅NO]₂[–] to form the initial product of nitroso and nitro compounds [69–71]. This mechanism permitted us to hypothesize that similar reactions would occur during exposure of enolic species to NO on Ag/Al₂O₃, resulting in the formation of organo–nitroso compound. Transformation of this organo–NO_x compound to its enol tautomer, –CH=N(OH), with subsequent dehydration to –CN and transformation to –NCO, has been proposed as a possible route for –NCO formation [45,56,72]. The presence of O₂ promoted the reaction of enolic species toward NO, possibly resulting in the formation of organo–nitro intermediate. These compounds were also relevant to produce –NCO via enol and –CNO formation [45,56,72].

Based on the above results, a simplified schematic model for the –NCO formation during the reduction of NO_x by ethanol over Ag/Al₂O₃ is shown in Fig. 9. In a typical reaction process, partial oxidation of ethanol results in the formation of enolic species adsorbed on Al and Ag sites, as well as the formation of acetate on Al sites. The enolic species intimately linked with Ag sites (RCH=CH–O–Ag and RCH=CH–O–Al–Ag), possessing high activity, further reacts with NO + O₂ (and/or NO), to form Ag–NCO. The enolic species adsorbed on Al sites (RCH=CH–O–Al, not shown in Fig. 9) and acetate bound on Al sites are less active when compared with the enolic species intimately linked with Ag sites and thus play a minor role in –NCO formation (Fig. 9). With an increase in the concentration of Ag–NCO, this species can transfer to Al sites, and as a result, the characteristic frequency of Al–NCO can be observed.

5. Conclusions

Ag species mainly present in the oxidized state, particularly in highly dispersed Ag⁺ ions on Ag/Al₂O₃, are active sites responsible for the reduction of NO_x by ethanol. Two kinds of surface enolic species, bound on or close to Ag (RCH=CH–O–Ag, RCH=CH–O–Al–Ag) and adsorbed only on Al sites (RCH=CH–O–Al), were identified by in situ DRIFTS and DFT calculations during the SCR of NO_x by ethanol over Ag/Al₂O₃ and Al₂O₃, respectively. The enolic species was preferably bound on or close to Ag sites, exhibiting an intimate contact with the active phase, which strongly suggests that highly dispersed Ag⁺ ions and oxidized silver clusters (Ag_n⁺) play a crucial role in surface enolic species formation during the reduction of NO_x by ethanol over Ag/Al₂O₃. The enolic species intimately

linked with Ag sites exhibits higher activity for reaction with NO + O₂ and/or NO to form –NCO species than that of the enolic species adsorbed on Al sites. During this reaction, furthermore, the consumption of enolic species intimately linked with Ag sites is fairly close to the formation of the final product N₂, quantitatively confirming its crucial role in the reduction of NO_x by ethanol over Ag/Al₂O₃. Surface acetate also formed during the partial oxidation of ethanol over Ag/Al₂O₃, while being prone to interaction with Al sites. This adsorption behavior of acetate may be responsible for its lower activity to produce –NCO when compared with the enolic species intimately linked with Ag sites. Thus, the major pathway for the reduction of NO_x by ethanol over Ag/Al₂O₃ involved the formation of enolic species bound on or close to Ag sites, which was followed by its transformation to –NCO (also intimately linked with the active phase); subsequently, –NCO reacted with NO + O₂ and/or nitrates to yield N₂.

Acknowledgments

This work was financially supported by the Special Co-construction Project of Beijing Municipal Commission of Education and the National Natural Science Foundation of China (21177142, 20973193, and 50921064).

Appendix A. Supplementary material

Supplementary data associated with this article can be found, in the online version, at <http://dx.doi.org/10.1016/j.jcat.2012.05.021>.

References

- [1] M. Iwamoto, H. Yahiro, Y. Yu-u, S. Shundo, N. Mizuno, *Shokubai (Catalyst)* 32 (1990) 430.
- [2] W. Held, A. König, T. Richter, L. Pupper, SAE Paper 900496, 1990.
- [3] A. Fritz, V. Pitchon, *Appl. Catal. B* 13 (1997) 1.
- [4] R. Burch, J.P. Breen, F.C. Meunier, *Appl. Catal. B* 39 (2002) 283.
- [5] H. He, Y.B. Yu, *Catal. Today* 100 (2005) 37.
- [6] M.A. Gómez-García, V. Pitchon, A. Kiennemann, *Environ. Int.* 31 (2005) 445.
- [7] Z. Liu, S. Ihl Woo, *Catal. Rev.* 48 (2006) 43.
- [8] K.-I. Shimizu, A. Satsuma, *Phys. Chem. Chem. Phys.* 8 (2006) 2677.
- [9] S. Roy, M.S. Hegde, G. Madras, *Appl. Energy* 86 (2009) 2283.
- [10] P.G. Savva, C.N. Costa, *Catal. Rev.* 53 (2011) 91.
- [11] P. Granger, V.I. Parvulescu, *Chem. Rev.* 111 (2011) 3155.
- [12] K.A. Bethke, H.H. Kung, *J. Catal.* 172 (1997) 93.
- [13] S. Sumiya, H. He, A. Abe, N. Takezawa, K. Yoshida, *J. Chem. Soc., Faraday Trans.* 94 (1998) 2217.
- [14] S. Kameoka, Y. Ukisu, T. Miyadera, *Phys. Chem. Chem. Phys.* 2 (2000) 367.
- [15] K. Shimizu, A. Satsuma, T. Hattori, *Appl. Catal. B* 25 (2000) 239.
- [16] A. Martínez-Arias, M. Fernández-García, A. Iglesias-Juez, J.A. Anderson, J.C. Conesa, J. Soria, *Appl. Catal. B* 28 (2000) 29.
- [17] L.E. Lindfors, K. Eränen, F. Klingstedt, D.Y. Murzin, *Top. Catal.* 28 (2004) 185.
- [18] Y.H. Yeom, M. Li, W.M.H. Sachtler, E. Weitz, *J. Catal.* 238 (2006) 100.
- [19] J.H. Lee, S.J. Schmiege, S.H. Oh, *Appl. Catal. A* 342 (2008) 78.
- [20] Y.F. Tham, J.Y. Chen, R.W. Dibble, *Proc. Combust. Inst.* 32 (2009) 2827.
- [21] V.I. Parvulescu, B. Cojocaru, V. Parvulescu, R. Richards, Z. Li, C. Cadigan, P. Granger, P. Miquel, C. Hardacre, *J. Catal.* 272 (2010) 92.
- [22] D.Y. Yoon, J.H. Park, H.C. Kang, P.S. Kim, I.S. Nam, G.K. Yeo, J.K. Kil, M.S. Cha, *Appl. Catal. B* 101 (2011) 275.
- [23] T. Miyadera, *Appl. Catal. B* 2 (1993) 199.
- [24] T. Chafik, S. Kameoka, Y. Ukisu, T. Miyadera, *J. Mol. Catal. A* 136 (1998) 203.
- [25] Y.H. Yeom, M. Li, W.M.H. Sachtler, E. Weitz, *J. Catal.* 246 (2007) 413.
- [26] A. Martínez-Arias, D. Gamarra, M. Fernández-García, A. Hornés, P. Bera, Z. Koppány, Z. Schay, *Catal. Today* 143 (2009) 211.
- [27] Y.B. Yu, H. He, Q.C. Feng, *J. Phys. Chem. B* 107 (2003) 13090.
- [28] Y.B. Yu, H. He, Q.C. Feng, H.W. Gao, X. Yang, *Appl. Catal. B* 49 (2004) 159.
- [29] Y.B. Yu, H.W. Gao, H. He, *Catal. Today* 93–95 (2004) 805.
- [30] M.K. Kim, P.S. Kim, J.H. Baik, I.-S. Nam, B.K. Cho, S.H. Oh, *Appl. Catal. B* 105 (2011) 1.
- [31] H. He, X.L. Zhang, Q. Wu, C.B. Zhang, Y.B. Yu, *Catal. Surv. Asia* 12 (2008) 38.
- [32] Q. Wu, H. He, Y.B. Yu, *Appl. Catal. B* 61 (2005) 107.
- [33] Q. Wu, H. Gao, H. He, *Chin. J. Catal.* 27 (2006) 403.
- [34] Y.B. Yu, X.P. Song, H. He, *J. Catal.* 271 (2010) 343.
- [35] A. Takahashi, M. Haneda, T. Fujitani, H. Hamada, *J. Mol. Catal. A* 261 (2007) 6.
- [36] Q. Yu, X. Wang, N. Xing, H. Yang, S. Zhang, *J. Catal.* 245 (2007) 124.

- [37] C.A. Taatjes, N. Hansen, A. McIlroy, J.A. Miller, J.P. Senosiain, S.J. Klippenstein, F. Qi, L.S. Sheng, Y.W. Zhang, T.A. Cool, J. Wang, P.R. Westmoreland, M.E. Law, T. Kasper, K. Kohse-Hoinghaus, *Science* 308 (2005) 1887.
- [38] H. He, C.B. Zhang, Y.B. Yu, *Catal. Today* 90 (2004) 191.
- [39] A. Musi, P. Massiani, D. Brouri, J.-M. Trichard, P. Da Costa, *Catal. Lett.* 128 (2009) 25.
- [40] A. Sultana, M. Haneda, T. Fujitani, H. Hamada, *Catal. Lett.* 114 (2007) 96.
- [41] K. Shimizu, M. Tsuzuki, K. Kato, S. Yokota, K. Okumura, A. Satsuma, *J. Phys. Chem. C* 111 (2007) 950.
- [42] S.T. Korhonen, A.M. Beale, M.A. Newton, B.M. Weckhuysen, *J. Phys. Chem. C* 115 (2011) 885.
- [43] X. She, M. Flytzani-Stephanopoulos, *J. Catal.* 237 (2006) 79.
- [44] P. Sazama, L. Capek, H. Drobna, Z. Sobalik, J. Dedecek, K. Arve, B. Wichterlova, *J. Catal.* 232 (2005) 302.
- [45] F.C. Meunier, J.P. Breen, V. Zuzaniuk, M. Olsson, J.R.H. Ross, *J. Catal.* 187 (1999) 493.
- [46] S. Chansai, R. Burch, C. Hardacre, J. Breen, F. Meunier, *J. Catal.* 276 (2010) 49.
- [47] T.E. Hoost, K.J. Kudla, K.M. Collins, M.S. Chattha, *Appl. Catal. B* 13 (1997) 59.
- [48] B. Wichterlová, P. Sazama, J.P. Breen, R. Burch, C.J. Hill, L. Čapek, Z. Sobalík, *J. Catal.* 235 (2005) 195.
- [49] L. Zhang, C. Zhang, H. He, *J. Catal.* 261 (2009) 101.
- [50] W.L. Johnson II, G.B. Fisher, T.J. Toops, *Catal. Today* 184 (2012) 166.
- [51] K. Shimizu, J. Shibata, H. Yoshida, A. Satsuma, T. Hattori, *Appl. Catal. B* 30 (2001) 151.
- [52] F.C. Meunier, V. Zuzaniuk, J.P. Breen, M. Olsson, J.R.H. Ross, *Catal. Today* 59 (2000) 287.
- [53] H.W. Gao, H. He, Y.B. Yu, Q.C. Feng, *J. Phys. Chem. B* 109 (2005) 13291.
- [54] Y. Ukisu, S. Sato, A. Abe, K. Yoshida, *Appl. Catal. B* 2 (1993) 147.
- [55] S. Kameoka, T. Chafik, Y. Ukisu, T. Miyadera, *Catal. Lett.* 55 (1998) 211.
- [56] N. Bion, J. Saussey, M. Haneda, M. Daturi, *J. Catal.* 217 (2003) 47.
- [57] N. Bion, J. Saussey, C. Hedouin, T. Seguelong, M. Daturi, *Phys. Chem. Chem. Phys.* 3 (2001) 4811.
- [58] F. Thibault-Starzyk, E. Seguin, S. Thomas, M. Daturi, H. Arnolds, D.A. King, *Science* 324 (2009) 1048.
- [59] S. Tamm, H.H. Ingelsten, A.E.C. Palmqvist, *J. Catal.* 255 (2008) 304.
- [60] R.M. Ferullo, M.M. Branda, G.R. Garda, N.J. Castellani, *J. Mol. Catal. A* 167 (2001) 115.
- [61] H. Gao, H. He, *Spectrochim. Acta A* 61 (2005) 1233.
- [62] J. Sirita, S. Phanichphant, F.C. Meunier, *Anal. Chem.* 79 (2007) 3912.
- [63] Y. Ukisu, T. Miyadera, A. Abe, K. Yoshida, *Catal. Lett.* 39 (1996) 265.
- [64] S. Sumiya, M. Saito, H. He, Q.C. Feng, N. Takezawa, K. Yoshida, *Catal. Lett.* 50 (1998) 87.
- [65] S. Chansai, R. Burch, C. Hardacre, J. Breen, F. Meunier, *J. Catal.* 281 (2011) 98.
- [66] J. Shen, R.D. Cortright, Y. Chen, J.A. Dumesic, *J. Phys. Chem.* 98 (1994) 8067.
- [67] M. Digne, P. Sautet, P. Raybaud, P. Euzen, H. Toulhoat, *J. Catal.* 211 (2002) 1.
- [68] H. Gao, T. Yan, Y. Yu, H. He, *J. Phys. Chem. C* 112 (2008) 6933.
- [69] D.L.H. Williams, in: V. Gold, D. Bethell (Eds.), *Advances in Physical Organic Chemistry*, vol. 19, Academic Press Inc., New York, 1983, p. 381.
- [70] R. Rathore, J.K. Kochi, *J. Org. Chem.* 61 (1996) 627.
- [71] M.B. Smith, J. March, *March's Advanced Organic Chemistry Reactions, Mechanisms, and Structure*, sixth ed., Wiley-Interscience A John Wiley & Sons Inc., 2007.
- [72] A. Obuchi, C. Wögerbauer, R. Köppel, A. Baiker, *Appl. Catal. B* 19 (1998) 9.